Hindawi Publishing Corporation
Discrete Dynamics in Nature and Society
Volume 2011, Article ID 487839, 11 pages
doi:10.1155/2011/487839

Research Article

The Multiscale Pore Connectivity Network via Scaling Relationship Derived from a Sandstone Image

Teo Lay Lian

Faculty of Engineering and Technology, Multimedia University, Melaka Campus, Jalan Ayer Keroh Lama, 75450 Melaka, Malaysia

Correspondence should be addressed to Teo Lay Lian, llteo@mmu.edu.my

Received 5 January 2011; Revised 31 March 2011; Accepted 28 May 2011

Academic Editor: B. Sagar

This paper presents a study on a multiscale pore connectivity network derived from a sandstone image. We first convert a grayscale sandstone image into pore and grain regions. The binary pore-grain image is transformed into multiscale pore by performing morphological opening operations with increasing structuring element size. A pore connectivity network (PCN), which is a skeleton network that describes the structure of pore space from multiscale pore-grain images, is extracted. The PCN can be computed by using morphological transformations with reference to three different probing rules (in the form of octagon, square, and rhombus). It is observed that the length of multiscale PCN varies with the number of opening transformations. This is due to the fact that the intricacy of the pore image is reduced with the increasing cycle of opening transformations. Next, we estimate the fractal dimensions of these multiscale PCNs using box-counting method. The values obtained follow universal power-law relationships. We further analyze the relationship of multidimensional opening in quantitative manner. A rescaled formula based on the linearity of decreasing fractal dimension values of pore space is proposed. This technique is applied to estimate the fractal dimensions of a sequence of multi-dimensional sandstone image generated by morphological opening.

1. Introduction

Pore space is formed due to random process of grain deposition, cementation, secondary geophysical and geochemical processes [1, 2]. Pore geometry and topological properties are related to processes of porous media formation. One of the efficient ways of characterizing processes of porous medium in a quantitative manner is by reducing the pore space into the connectivity network [3, 4]. In order to understand the properties of material, it is thus

essential to study the effect of the connectivity network models in material. Pore network models are mechanistic models that idealize the complex geometry of the porous media by representing the pore space with pore elements having simple geometric shapes. These network models are effective tools to investigate or predict macroscopic properties from fundamental pore scale behavior or processes and phenomena that are difficult to obtain experimentally. Typical properties of network model include the network topology in which pore connects a subset of the network geometry consisting of pore locations and volumes and channel cross-sectional areas. Geometrical simplifications of pore and channel shapes are often implicitly built into these models [4]. The most critical part in constructing a pore network model is defining its structure and geometry. To overcome this problem, various representations of pore network models have been proposed to provide more realistic description of the connectivity by defining pore-throat length distribution, pore-body size distributions, throat-body size distribution, and the spatial correlation between pore bodies and pore throats [5]. Due to the complexity of pore space morphology, pore bodies are usually represented by simplified shapes such as spheres, cubes, or prisms, while pore throats are represented by circular, rectangular, or triangular cross-section.

Several theoretical attempts have been made to deal with characterization of rock through geometrical descriptors and fractal analysis of pore space. Vogel and Roth [3] generated a pore network model based on pore-size distribution and connectivity function obtained by calculating three-dimensional Euler number. The pore size distribution is obtained by a series of erosion-dilation algorithm. On the other hand, Bird and Perrier [6] have developed a fractal approach to model variations in soil bulk density and porosity with scale of measurement or sample size. Most common network models are either cubic lattices with restricted connectivity or random pore network models with variable connectivity generated to provide more realistic representation of the pore space of the porous media. Perrier et al. [7] have proposed pore-solid fractal (PSF) model, which is a multiscale model of porous medium. They described the fractal approach to model soil structure, in which a range of particles and pore sizes are incorporated in common geometric model.

In this paper, a multiscale structure of pore space is obtained by morphological opening process using three different structuring elements. Classically, the process of multiscale-dimensional pore images begins with the morphological opening technique by smoothing and reducing the dimension of pore images [8, 9]. The multiscale approach leads to the stabilized structuring elements used in opening transformations, which prevent the excessive differences of area of opening process introduced in the pore space.

The outline of this paper is shown as follows. The techniques of morphological transformations are employed to generate multiscale pore space and, further, to extract the pore connectivity networks. A mathematical formulation is proposed to investigate the fractal properties of pore connectivity networks. It is observed that the fractal dimension of pore space decreases with the increasing opening process. Lastly, we show the fractal power-law relationship based on number-decomposed network relationship.

2. Morphological Transformations

Mathematical morphology is a technique for the analysis and processing of geometrical structures. Mathematical morphology was originally developed for binary images and was later extended to grayscale images. In binary morphology, an image (M) is *probed* with a simple, specific shape, called structuring element (S) to examine how well this shape fits into

the image under test. There are four basic morphological transformations namely: *dilation*, *erosion*, *opening*, and *closing* [8, 9].

Dilation:

$$M \bigoplus S = \{m + s : m \in M, s \in S\} = \bigcup_{s \in S} M_s. \tag{2.1a}$$

Erosion:

$$M \ominus S = \{m - s : m \in M, s \in S\} = \bigcap_{s \in S} M_s. \tag{2.1b}$$

Opening:

$$M \circ S = (M \ominus S) \bigoplus S. \tag{2.1c}$$

Closing:

$$M \bullet S = \left(M \bigoplus S\right) \ominus S. \tag{2.1d}$$

Dilation and erosion are, respectively, useful to enlarge and shrink an image to a desired degree and direction by toning the characteristic of structuring elements. On the other hand, cascaded erosion-dilation or dilation-erosion operations are commonly employed to smoothen an image [8, 9].

In this paper, a sandstone microphotograph obtained by a scanning electron microscope (SEM) is considered. The sandstone image has 480 × 480 pixels, in grayscale (0–255) levels (Figure 1(a)). By using a simple thresholding technique, the grayscale sandstone image is converted to a binary pore space (black) and grain (white) regions (Figure 1(b)). Morphological operations are then applied to transform this binary pore. Three basic structuring elements S are considered here, namely, rhombus (Figure 2(a)), square 3×3 (Figure 2(b)), and octagon (Figure 2(c)). Multiscale pore space (Figures 3(a)–3(j)) is first generated by performing 10 cycles of multiscale opening on the pore space, which is in fact the multiscale closing of grain. Based on a sequence of multiscale pore images (Figure 3), it is obvious that the pore region is gradually reduced with increasing cycle of structuring template.

3. Pore Connectivity Network: Skeletonisation Transformation

In this section, a systematic approach is applied to extract the pore connectivity network (PCN) from multiscale pore-space of sandstone image. The PCNs can be extracted by implementing a skeletonization process where the basic morphological transformations are systematically employed as shown in

$$\mathrm{PCN}_n(M) = (M \ominus kS) - [(M \ominus kS) \circ S] \quad k = 1, 2, \ldots N. \tag{3.1}$$

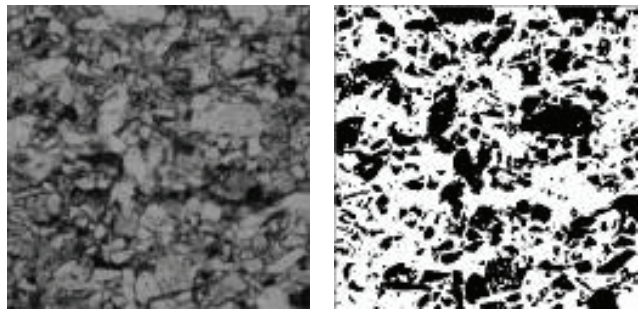

(a) (b)

Figure 1: (a) The grayscale sandstone image obtained by SEM. (b) The binary pore image (black and white colors represent grains and pore spaces, resp.).

$$\begin{array}{ccc} & & 1\,1\,1 \\ & & 1\,1\,1\,1\,1 \\ 1 & 1\,1\,1 & 1\,1\,1\,1\,1 \\ 1\,1\,1 & 1\,1\,1 & 1\,1\,1\,1\,1 \\ 1 & 1\,1\,1 & 1\,1\,1 \end{array}$$

(a) (b) (c)

Figure 2: The structure templates of (a) rhombus, (b) square 3×3 and (c) octagon.

In the above expression, the $\mathrm{PCN}_n(M)$ denotes the nth pore network subsets of pore (M). Subtracting from the eroded version of M, the morphological opening by structuring elements retains only the angular points, which are the connectivity points or subsets in this model. The union of all such possible network subsets produces the $\mathrm{PCN}_n(M)$. The structuring elements used in this network extraction are rhombus, square 3×3, and octagon. By combining these decomposed network subsets via logical union, PCNs are formed. This operation can be mathematically defined as

$$\mathrm{PCN}(M) = \bigcup_{n=0}^{N} \mathrm{PCN}_n(M). \tag{3.2}$$

Based on the PCN extraction procedure explained above, we transform all the multiscale images (Figures 3(a)–3(j)) into their PCNs by means of three structuring elements. Figures 4(a)–4(j) illustrate the extracted PCN by rhombus, square $\mathbf{3} \times \mathbf{3}$, and octagon, respectively. Less intricacy of connectivity networks is observed in higher opening cycles of model images. This is due to decreasing number of the small-diameter circles in pore space at higher opening process, and hence, lesser intricate connectivity networks are formed. It is also observed that the connectivity networks formed by octagon and square $\mathbf{3} \times \mathbf{3}$ are more bounded, but are thicker in widths. As for the rhombus, although the appearance of the network connectivity shown in branched forms, some parts are disconnected (Figures 4(a)(i)–4(j)(i)) and are thinner in widths. Therefore, it may be misleading that the connectivity formed by rhombus generally provides finer network information at lower dimensions as compared to the thicker connectivity networks formed by square $\mathbf{3} \times \mathbf{3}$ and

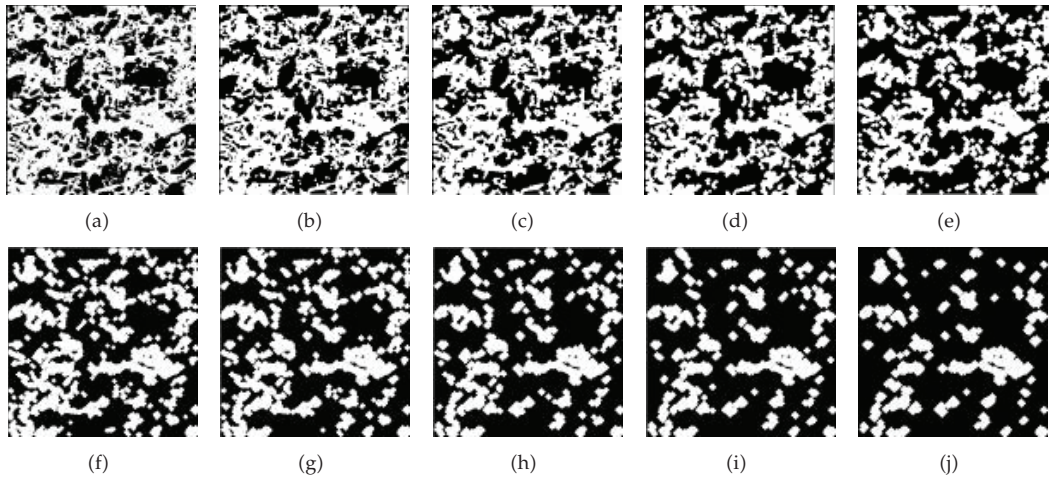

Figure 3: (a–j) A sequence of multiscale pore generated via opening transformations by a symmetric rhombus.

octagon. However, less bounded network forms are observed at higher opening of pore images.

In order to understand the characterization of networks formed by different structuring elements on multiscale pore space, it is essential to estimate the length of PCNs in multidimensional spaces. It is also important to indicate what kind of shape or structuring element is employed to extract PCNs. The latter influences the PCN pattern. With the increasing cycles of opening on pore space, it is reasonable to expect that less branched PCNs formed due to the decreasing number of smaller grains as the opening transformation was applied on pore space.

To characterize the connectivity networks, we measure their fractal properties. To obtain the fractal properties of this network, the lengths of PCNs at their respective scale in pixel units are computed. The fractal dimensions of these multiscale connectivity networks can then be obtained by box-counting method. Figures 5(a)–5(j) illustrate the relationship of the multiscale PCNs of a pore space. Figure 5(k) summarizes the estimated fractal dimension for rhombus, square 3×3, and octagon at 1–10 iterations of opening process. Their corresponding values are presented in Table 1.

The fractal values in Table 1 range between 1.1–1.7, suggesting that the PCNs do not fall in a single universality class; it however depends on the surface area provided. From these results, it is possible to define a variety of interesting topological properties of connectivity networks formed in pore space. These fractal dimension values confirm with the values arousing from our previous study [10]. The fractal dimensions have decreasing trends with the increasing cycle of opening transformation as shown in Table 1. Fractal dimensions obtained for the connectivity networks extracted by rhombus at higher cycle of opening are smaller than the square 3×3 and octagon. However, the fractal dimension of the networks extracted by octagon is higher than that of square 3×3 and rhombus at higher iterations of opening.

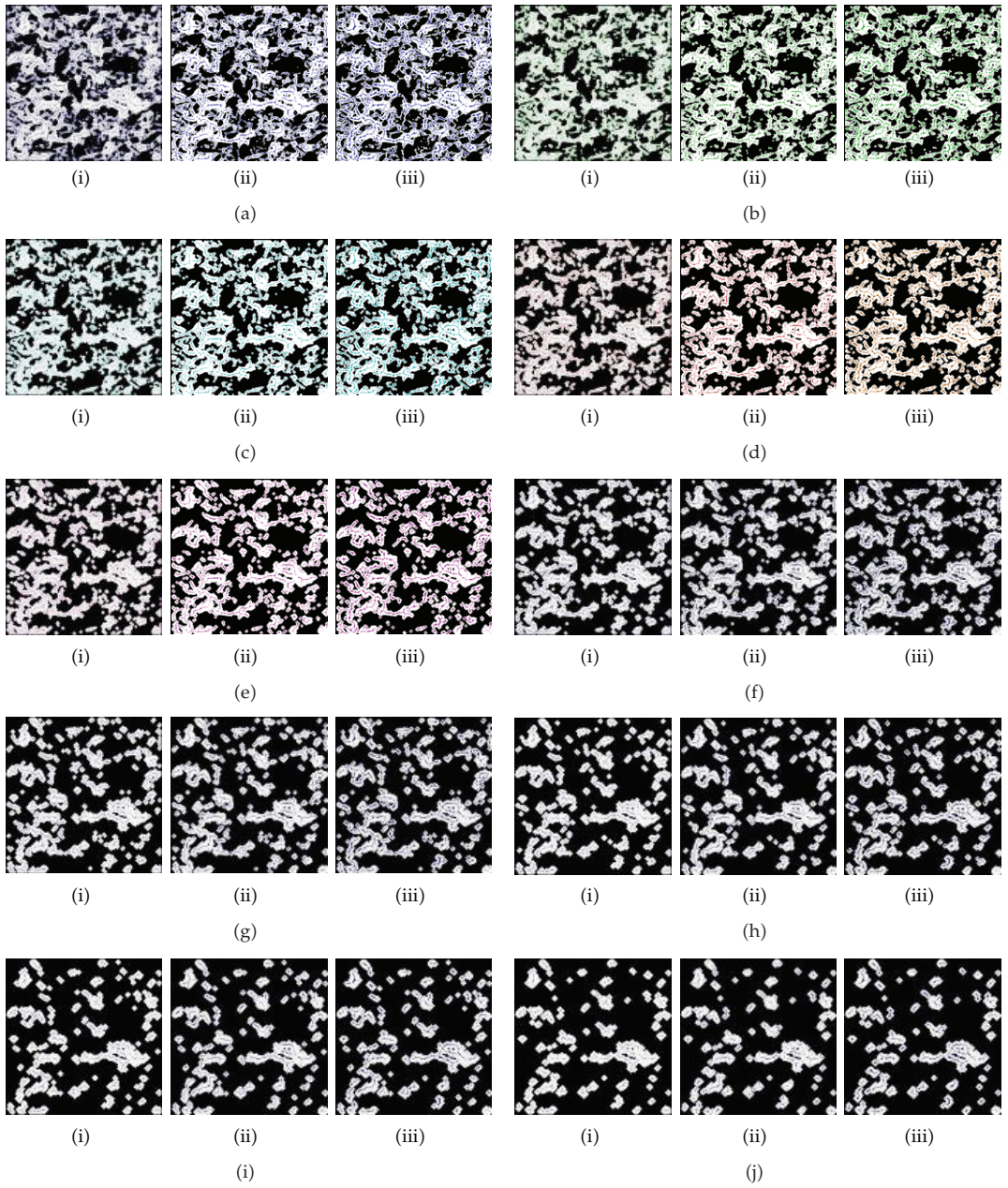

Figure 4: (a–j) The opening transformations of pore images in Figure 3(a)–3(j) are used to extract pore connectivity networks by structuring elements ((i) rhombus, (ii) square, and (iii) octagon).

Let M be a class of topology open set on Euclidean space, Z^2, and let $X \in M$ be an open nonempty space. The spatial of this set is the space to be opened by mathematical morphology transformation.

$$X_I, X_2, X_3, \ldots X_n \in M. \tag{3.3}$$

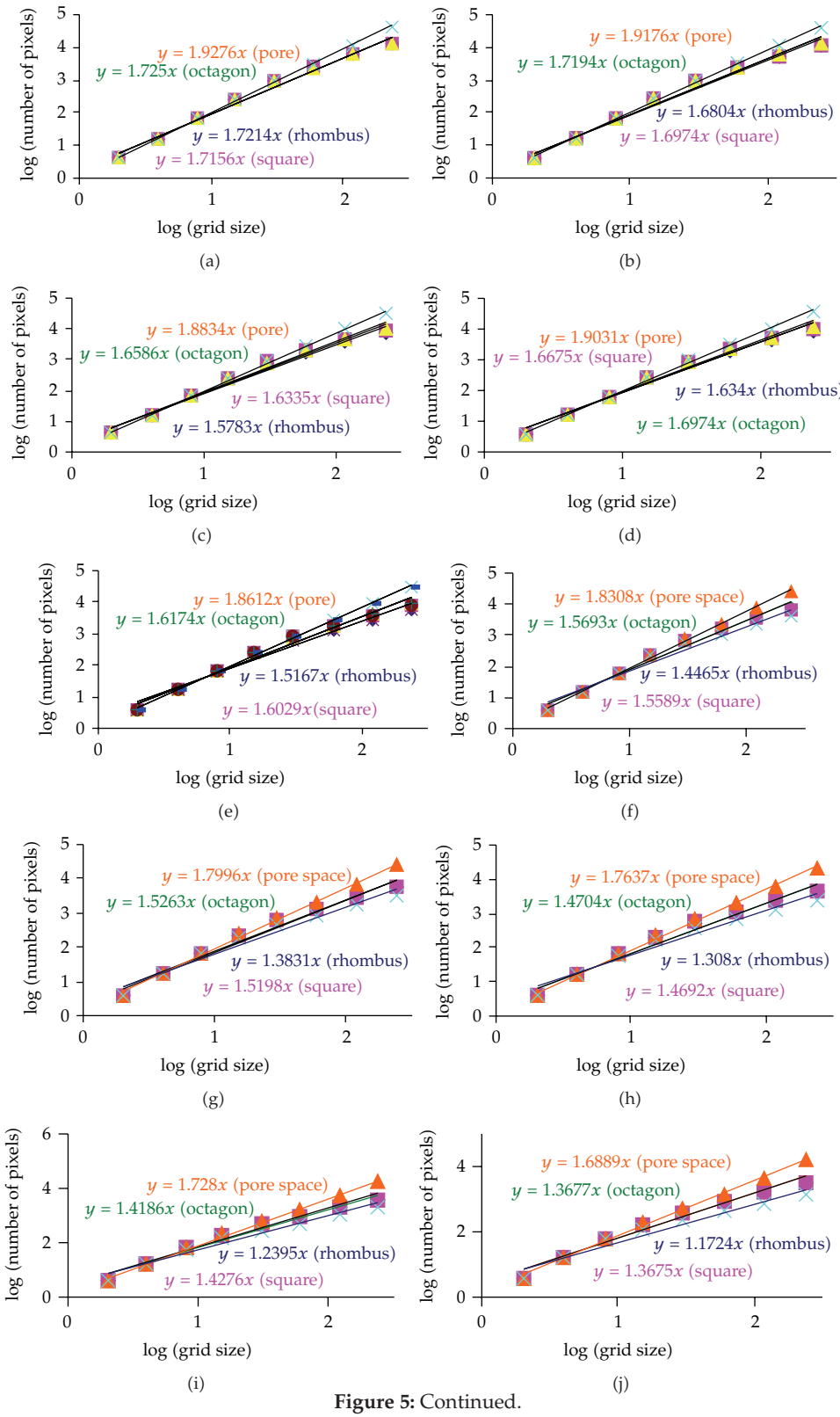

Figure 5: Continued.

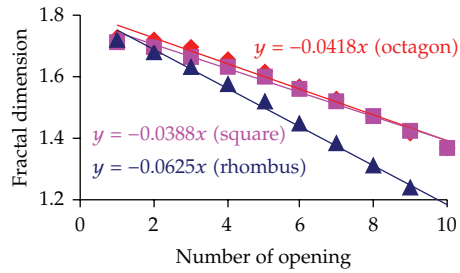

(k)

Figure 5: (a–j) Graphical plots between log (number of pixels of pore connectivity network formed by structuring elements ((i) rhombus, (ii) square, (iii) octagon or pore space) versus log (step sizes) from the first to the tenth iterations of opening process and (k) the fractal dimension for three structuring elements.

Table 1: Fractal dimension estimation on pore connectivity networks and pore space by using box-counting method.

Number	Fractal Dimension (D_f)			
	Pore space (opening)	*Opening* (pore connectivity network)		
		Rhombus	Square	Octagon
1	1.9276	1.7214	1.7156	1.7250
2	1.9176	1.6804	1.6974	1.7194
3	1.9031	1.6340	1.6675	1.6974
4	1.8834	1.5783	1.6335	1.6586
5	1.8612	1.5167	1.6029	1.6174
6	1.8308	1.4465	1.5589	1.5693
7	1.7996	1.3831	1.5198	1.5263
8	1.7637	1.3080	1.4692	1.4704
9	1.7280	1.2395	1.4276	1.4186
10	1.6889	1.1724	1.3675	1.3677
15	1.4561	0.7960	1.1202	1.0808

When the opening is performed on the pore space, smaller particles in the open nonempty space disappear and hence the remaining space is smoother. Let R be the connectivity network formed in the open nonempty space. When the space is smoothen and less small particles are opened, the network connectivity will be reduced since opening transformations (p_i) and less intricate networks will be formed. X_i at i-times of opening process will form network connectivity (R_i), as shown below:

$$\begin{aligned} X_1 &= M \text{ with one times of opening process} && (p_1) \sim R_1 \\ X_2 &= M \text{ with two times of opening process} && (p_2) \sim R_2 \\ X_3 &= M \text{ with three times of opening process} && (p3) \sim R_3 \\ &\vdots && \vdots \\ X_n &= M \text{ with } n \text{ times of opening process} && (p_n) \sim R_n. \end{aligned} \tag{3.4}$$

Table 2: The reduction factor by opening process in Figure 5(k).

Reduction Factors Pore space—opening (m_i)	Connectivity networks		
	Rhombus	Square 3 × 3	Octagon
Sandstone	0.0625	0.0388	0.0418

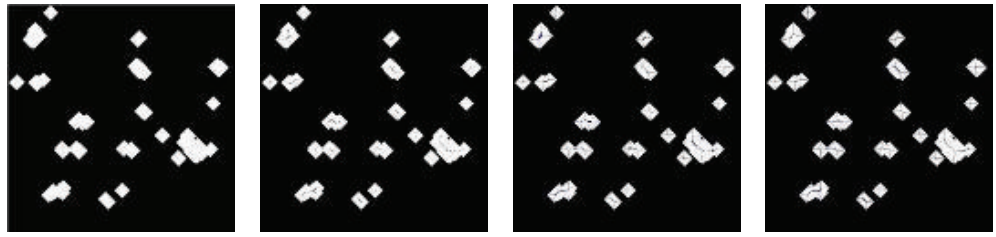

(a) (b) (c) (d)

Figure 6: (a) Fifteen times of opening transformations applied at binary pore space; (b–d) opening image of (a) is used to extract pore connectivity networks of structuring elements ((i) rhombus, (ii) square, and (iii) octagon).

The lengths of connectivity network are reduced due to the increasing cycle of opening process (p_i), and as a result, less branched networks are observed. While measuring the relative results of fractal (D_i) with opening transformations (p_i), it is observed that the decreased graphical plots in Figure 5(k) for different types of structuring elements can be rescaled appropriately. Therefore, it is proposed that

$$D_i = m_i(p_i - 1) + D_1, \quad m_i < 1. \tag{3.5}$$

The gradient m_i is obtained from the regression plot of Figure 5(k) for different types of structuring elements, and D_1 is the fractal dimension of the first opening transformation.

$$m_i = \text{gradient } (D_{1,2,\ldots,n},\ P_{1,2,\ldots,n}). \tag{3.6}$$

The empirical values of m_i for the rhombus, square, and octagon are presented in Table 2.

We now address the question whether relation (3.5) can be regarded as a general property to predict the subsequent fractal dimensions without performing opening transformation. We applied this formula to estimate the fractal dimension of successive opening. We choose arbitrarily 15 times of opening transformations as shown in Figure 6(a). Same structuring elements (rhombus, square 3 × 3, and octagon) are employed to extract the corresponding PCNs (Figures 6(b)–6(d)). After the 15th cycle of opening transformation, the calculated values of fractal dimension D_{15} are 0.846, 1.172, and 1.140, respectively, as compared to the experimental results of 0.796, 1.120, and 1.081. The differences are less than 6%. This comparison shows the significance of the scaling exponent that we derive from this multiscale analysis of PCN via fractal dimension.

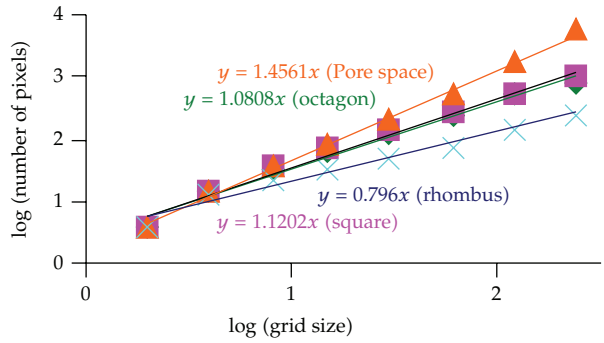

Figure 7: Graphical plots between log (number of pixels of pore connectivity network in Figure 6(a)–6(c) by structuring elements ((i) octagon, (ii) square or pore space) versus log (step sizes) from the first to the tenth iterations of opening process.

4. Conclusions

Analysis of pore connectivity network is addressed in this paper. A grayscale microphotograph of a sandstone sample is considered. The pore connectivity networks at multidimensional pore space are extracted via mathematical morphology transformations. We investigate the characterization of pore connectivity networks by estimating the fractal dimension of each connectivity network.

A model that is capable of describing the characterization of connectivity networks is developed. The decreasing trend in the smaller category of pore model reveals a strong influence of the fractality in this system. This gives a clear indication that one must characterize the possible self-similar fractal of model space in order to understand its behavior under different dimensions of surface area. The modeling techniques employed here can provide some interesting information to characterize the complicated network pattern problems. For example, our results show that the fractal dimensions of the network models decrease as the effect of multiscale opening transformations. Another interesting result is that the fractal dimension of connectivity network formed by rhombus at higher opening process is lesser than those of the square 3×3 and octagon. We believe that this might intimately be related to the characterization of lengths of connectivity networks by these three structuring elements. The fractal dimension of pore connectivity network exhibits a linear scaling distribution with opening processes of pore space image. The sandstone pore space possesses a simple relationship between the fractal dimension and the porosity of the rock as also opined by Mandelbrot [11]. The power-law relationship is observed in this pore space decomposition by means of octagon, rhombus, and square structuring elements:

$$N(r) \propto r^{-\alpha} \quad \text{with } D = \alpha - 1, \tag{4.1}$$

where N, r, α, and D are, respectively, the number of pixels of pore connectivity network, size of structuring elements, slope of the regression line, and fractal dimension.

Furthermore, it is found that the fractal dimensions of the pore connectivity network for square and octagon are deceased in scaling plots as increasing the opening processes. We introduced a rescaled formula based on the linearity of decreasing values fractal dimension

of pore space. This proposed formulation to estimate fractal dimension has been verified by experimental data.

Acknowledgment

The author gratefully acknowledges the support from the excellent computational facilities provided by the Multimedia University, Malaysia.

References

[1] R. Hellmann, P. J. N. Renders, J. P. Gratier, and R Guiget, "Experimental pressure solution compaction of chalk in aqueous solutions. Part 1. Deformation behavior, and chemistry," in *Water-Rock Interactions, Ore Deposits, and Environmental Geochemistry: A Tribute to David A. Crerar*, no. 7, pp. 129–152, Special Publication, 2002.

[2] R. Hellmann, P. Gaviglio, P. J. N. Renders, J. P. Gratier, S. Bekri, and R Guiget, "Experimental pressure solution compaction of chalk in aqueous solutions. Part 2. Porosimetry, synthetic permeability, and X-ray computerized tomography," in *Water-Rock Interactions, Ore Deposits, and Environmental Geochemistry: A Tribute to David A. Crerar*, pp. 153–178, 2002.

[3] H. J. Vogel and K. Roth, "Quantitative morphology and network representation of soil pore structure," *Advances in Water Resources*, vol. 24, no. 3-4, pp. 233–242, 2001.

[4] H. J. Vogel, "A numerical experiment on pore size, pore connectivity, water retention, permeability, and solute transport using network models," *European Journal of Soil Science*, vol. 51, no. 1, pp. 99–105, 2000.

[5] M. A. Celia, P. C. Reeves, and L. A. Ferrand, "Pore-scale models for multiphase flow in porous media," *Reviews of Geophysics*, vol. 33, no. 2, pp. 1049–1057, 1995.

[6] N. R. A. Bird and E. M. A. Perrier, "The pore-solid fractal model of soil density scaling," *European Journal of Soil Science*, vol. 54, no. 3, pp. 467–476, 2003.

[7] E. Perrier, N. Bird, and M. Rieu, "Generalizing the fractal model of soil structure: the PSF approach," *Geoderma*, vol. 88, no. 3-4, pp. 137–164, 1999.

[8] J. Serra, *Image Analysis andMathematical Morphology*, Academic Press, London, UK, 1982.

[9] J. Serra, *Image Analysis and Mathematical Morphology: Theoretical Advances*, vol. 2, Academic Press, London, UK, 1988.

[10] L. L. Teo, P. Radhakrishnan, and B. S. Daya Sagar, "Morphological decomposition of sandstone pore-space: fractal power-laws," *Chaos, Solitons and Fractals*, vol. 19, no. 2, pp. 339–346, 2004.

[11] B. B. Mandelbrot, *The Fractal Geometry of Nature*, W. H. Freeman, New York, NY, USA, 1983.